

**Temperature and Doping-Tuned Coordination Environments around
Electroactive Centers in Fe-doped $\alpha(\beta)$ -Ni(OH)₂ for Excellent Water
Splitting**

Qinghe Cao,^a Mi Luo,^b Yutian Huang,^a Qi Liu,^a Xiaoxing Kong,^a Jinlong Lei,^a Zheng Jiang^{*b} and Jiahai Wang^{*a}

^a Department of Chemistry and Chemical Engineering, Guangzhou Key Laboratory for Environmentally Functional Materials and Technology, Guangzhou University, Guangzhou 510006, P.R. China. E-mail: jiahaiwang@gzhu.edu.cn

^b Shanghai Synchrotron Radiation Facility, Zhangjiang National Lab, Shanghai Advanced Research Institute, Chinese Academy of Sciences, Shanghai 201204, PR. China. E-mail: jiangzheng@zjlab.org.cn

Experimental Section

Materials:

Ethanol, hydrochloric acid, potassium hydroxide, acetone, nickel(II) nitrate hexahydrate, iron(III) nitrate nonahydrate and urea were purchased from the Sinopharm Chemical Reagent Co., Ltd. Pt/C (20 wt% Pt) was purchased from the Shanghai Macklin Biochemical Co., Ltd. Nickel foam was obtained from the KunShan Kunag Xun Electronics Co., Ltd. RuO₂ was purchased from Aladdin Ltd. All of the reagents are of AR grade and were directly used in the experiments.

Synthesis of Fe-doped Ni(OH)₂ on Ni Foam:

Before the reaction, Ni foam (20 mm × 35 mm × 1 mm in size) was pretreated with acetone and 3 M HCl with 15 minutes of sonication. To synthesize the Fe-doped Ni(OH)₂, Ni(NO₃)₂·6H₂O (0.194 g), Fe(NO₃)₃·9H₂O (0.539 g) and urea (0.3 g) were dissolved in 35 mL of H₂O. Then, the yellow solution along with the above-cleaned Ni foam was put into an autoclave (50 mL). The sealed autoclave was heated to 120 °C (180 °C, 240 °C) for 10 h. The synthesis of Ni(OH)₂ nanosheets had analogous procedures except for not adding Fe(NO₃)₃·9H₂O. The synthesis of NiO had analogous procedures except that the heating temperature was increased to 280 °C.

Characterization:

The instrument used for SEM was a field emission scanning electron microscope (SU8010). The XRD data was obtained from a Bruker D8 ADVANCE Diffractometer ($\lambda=1.5418 \text{ \AA}$). TEM and HRTEM were performed on a JEM-2100 with an accelerating voltage of 200 kV. The instrument used for XPS was a Thermo Scientific

Escalab 250Xi. Raman spectroscopy was conducted with an excitation wavelength of 514 nm. X-ray absorption spectra at the K-edges of Ni and Fe were measured in the transmission mode at beamline BL14W1 at the Shanghai Synchrotron Radiation Facility (SSRF, China). The synchrotron beam of BL14W1 was monochromatized using a double-crystal monochromator (DCM) operated at 3.5 GeV. The beam size at the sample was approximately 300 um×300 um (FWHM). All of the XAFS spectra were averaged from 2 scans and were analyzed using the Demeter software package (University of Chicago).

Electrochemical measurements:

Fe-doped Ni(OH)₂ prepared in this experiment is directly used as the working electrode. A saturated calomel electrode and graphite rod were used as reference electrode and counter electrode, respectively. The current density was calculated based on the geometric area of the electrode. All potentials used in this study are versus the reversible hydrogen electrode (RHE): $E(\text{RHE}) = E(\text{SCE}) + 0.0591\text{pH} + 0.2415 - 0.000761(T - 298.15)$. Electrochemical impedance spectroscopy (EIS) was performed in a frequency range of 100 KHz to 1 Hz (amplitude 5 mV).

DFT calculations:

First-principle calculations were performed by the density functional theory (DFT) using the Vienna Ab-initio Simulation Package (VASP) package. The generalized gradient approximation (GGA) with the Perdew–Burke–Ernzerhof (PBE) functional was used to describe the electronic exchange and correlation effects. Uniform G-centered k-point meshes with a resolution of $2\pi * 0.03 \text{ \AA}^{-1}$ and Methfessel-Paxton

electronic smearing were adopted for the integration in the Brillouin zone for geometric optimization. The simulation was run with a cutoff energy of 500 eV throughout the computations. These settings ensure convergence of the total energies to within 1 meV per atom. Structural relaxation proceeded until all forces on atoms were less than 1 meV Å⁻¹ and the total stress tensor was within 0.01 GPa of the target value.

The bulk surface structures of β-Ni(OH)₂ (101), Fe-doped β-Ni(OH)₂ (101) and Fe-doped α-Ni(OH)₂ (012) were constructed with periodic boundary conditions and a gamma-point mesh of 3 × 2 × 1, which also included a 15 Å vacuum perpendicular to the surface. The free energy of the adsorption atomic hydrogen (ΔG_{H^*}) is obtained as follows:

$$\Delta G_{H^*} = \Delta E_{H^*} + \Delta E_{ZPE} - T\Delta S_{H^*}$$

ΔE_{H^*} describes the energy needed to increase the coverage by one hydrogen atom. ΔE_{ZPE} is the difference in the zero point energy, and ΔS_{H^*} is the difference in entropy. $\Delta E_{ZPE} - T\Delta S_{H^*}$ is approximately 0.24 eV, and thus, $\Delta G_{H^*} = \Delta E_{H^*} + 0.24$. For ΔE_{H^*} , it is calculated as follows:

$$\Delta E_{H^*} = E(\text{surface}+H) - E(\text{surface}) - 1/2 E(H_2)$$

where $E(\text{surface}+H)$ represents the total energy of the Ni(OH)₂ surface with one adsorbed hydrogen atom on the surface, $E(\text{surface})$ represents the total energy of the unmodified/modified Ni(OH)₂ surfaces, while $E(H_2)$ represents the total energy of a gas phase H₂ molecule.

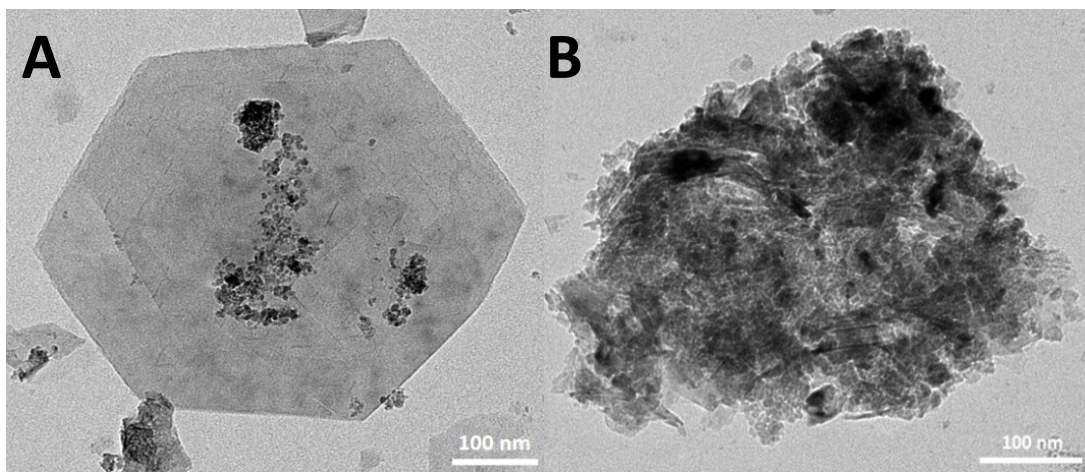


Figure S1 Low-resolution TEM images of A) Fe-doped α -Ni(OH)₂-120 and B) Fe-doped β -Ni(OH)₂-240.

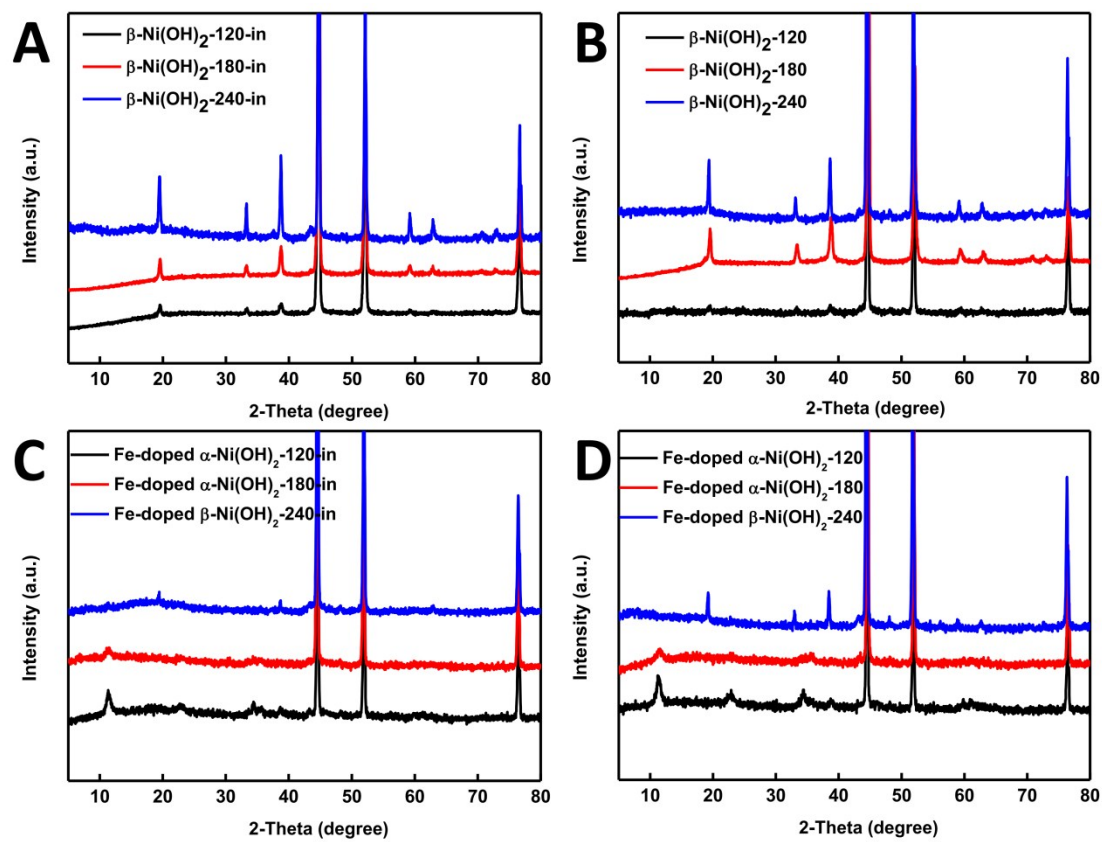


Figure S2 XRD patterns of Ni(OH)₂ prepared by the hydrothermal treatment of A) pure NF, B) NF with $\text{Ni}(\text{NO}_3)_2$ added, C) NF with $\text{Fe}(\text{NO}_3)_3$ added and D) NF with $\text{Ni}(\text{NO}_3)_2$ and $\text{Fe}(\text{NO}_3)_3$ added at 120, 180 and 240 °C, respectively (“in” represents no $\text{Ni}(\text{NO}_3)_2$ or $\text{Fe}(\text{NO}_3)_3$ added).

Table 1 The influence of temperature and Fe-doping on the phase change of Ni(OH)₂.

Sources \ Temperature (°C)	NF	NF+Ni(NO ₃) ₂	NF+Fe(NO ₃) ₃	NF+Ni(NO ₃) ₂ +Fe(NO ₃) ₃
120	β-Ni(OH) ₂	β-Ni(OH) ₂	Fe-doped α-Ni(OH) ₂	Fe-doped α-Ni(OH) ₂
180	β-Ni(OH) ₂	β-Ni(OH) ₂	Fe-doped α-Ni(OH) ₂	Fe-doped α-Ni(OH) ₂
240	β-Ni(OH) ₂	β-Ni(OH) ₂	Fe-doped β-Ni(OH) ₂	Fe-doped β-Ni(OH) ₂

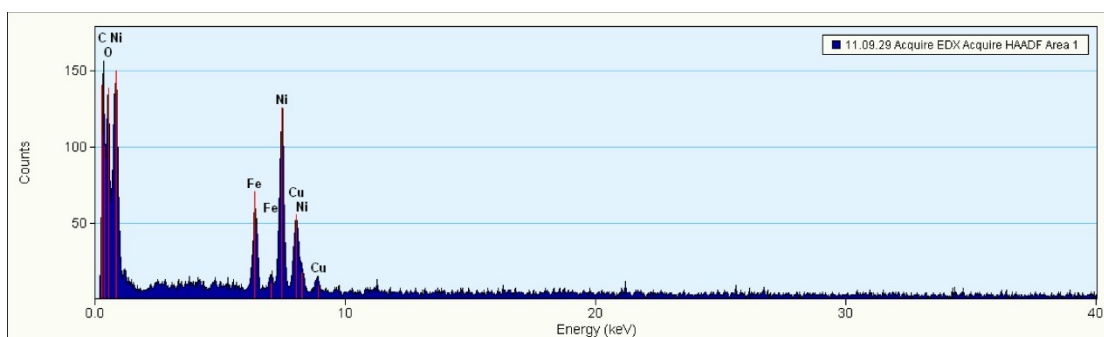


Figure S3 TEM-EDS spectra of Fe-doped α-Ni(OH)₂-120.

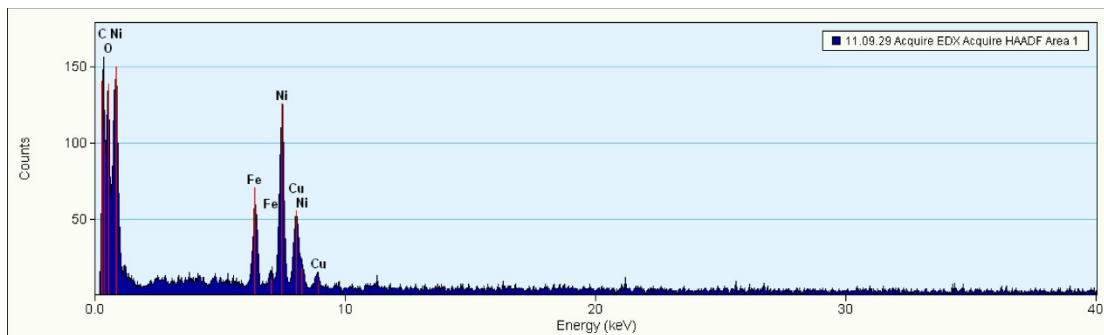


Figure S4 TEM-EDS spectra of Fe-doped β-Ni(OH)₂-240.

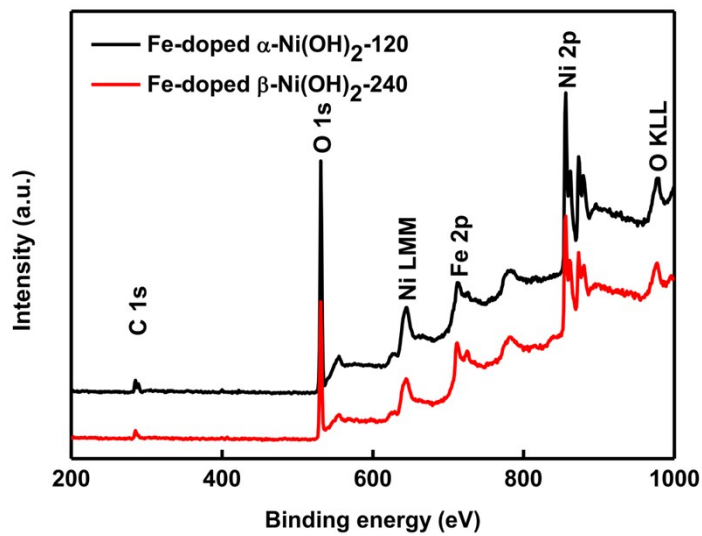


Figure S5 XPS full spectra of Fe-doped α -Ni(OH)₂-120 and Fe-doped β -Ni(OH)₂-240.

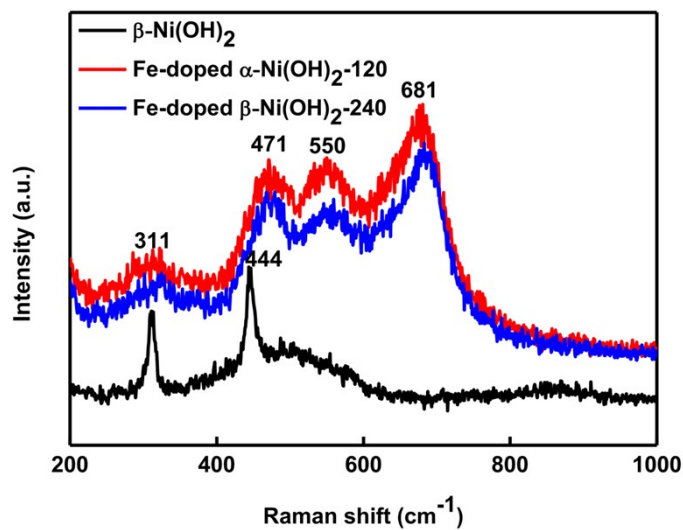


Figure S6 Raman spectra of β -Ni(OH)₂, Fe-doped α -Ni(OH)₂-120 and Fe-doped β -Ni(OH)₂-240.

Table S2 Comparisons of OER performances of Fe-doped α -Ni(OH)₂-120 with other

non-precious metal OER catalysts in 1.0 M KOH.

Catalysts	j (mA cm $^{-2}$)	Overpotential (mV)	Ref.
CoNi(OH) $_x$	10	280	1
NiFeOF	10	295	2
Fe-CoP	10	230	3
α -NiOOH	10	266	4
Fe-doped NiPS $_3$	30	256	5
NiFe LDH@NiCoP	10	220	6
Ni $_3$ FeN	10	280	7
Ni $_3$ S $_2$	10	223	8
Fe-Ni $_3$ C	10	275	9
Fe-doped α -Ni(OH) $_2$ -120	10/30	208/223	This work

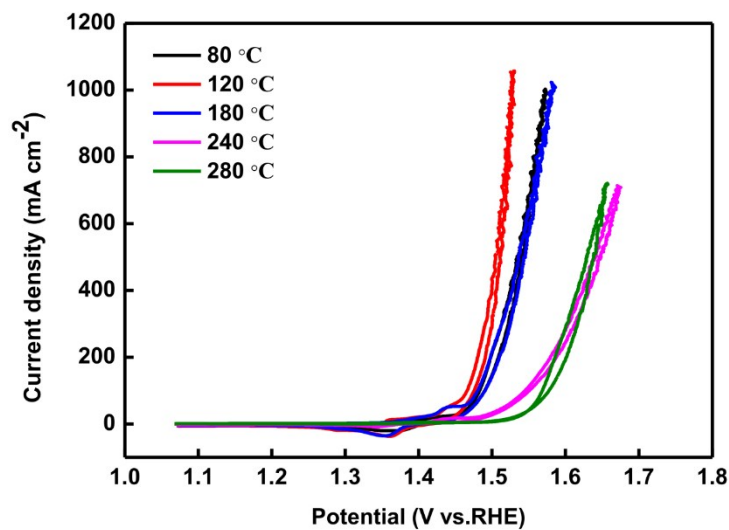


Figure S7 CV curves of samples prepared at different temperatures. The best OER performance is obtained at 120 °C.

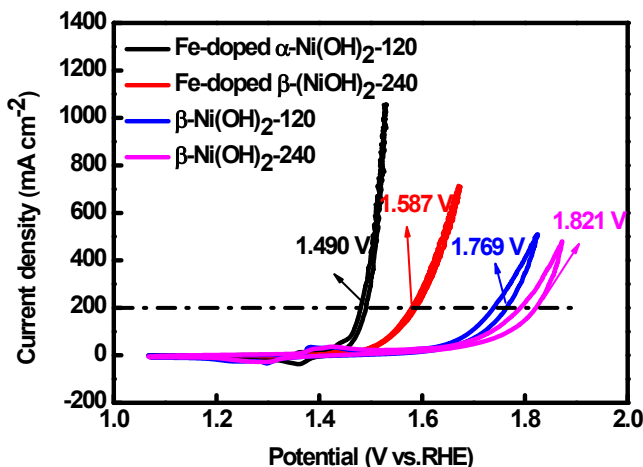


Figure S8 CV curves of Fe-doped α -Ni(OH)₂-120, Fe-doped β -Ni(OH)₂-240, β -Ni(OH)₂-120 and β -Ni(OH)₂-240.

Table S3 The comparison of overpotential (V vs.RHE) required to reach a current density of A) 200 mA cm⁻² and B) 300 mA cm⁻² for Ni(OH)₂ prepared in different conditions.

A:

Temperature (°C)	Catalysts	Ni(OH) ₂	Fe-doped Ni(OH) ₂
120		0.539	0.260
180		0.551	0.280
240		0.591	0.357

B:

Temperature (°C)	Catalysts	Ni(OH) ₂	Fe-doped Ni(OH) ₂
120		0.561	0.270
180		0.582	0.294
240		0.617	0.383

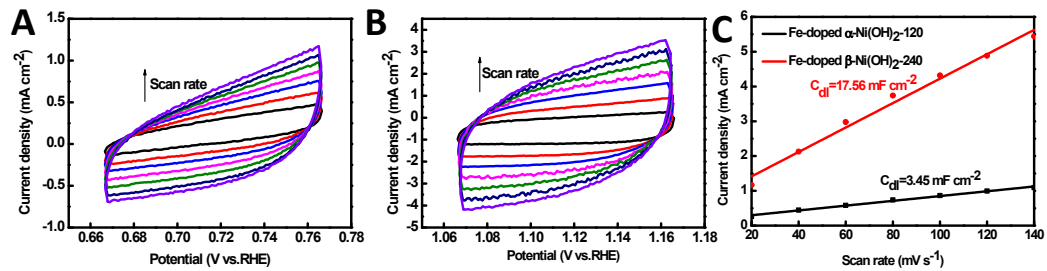


Figure S9 CV curves of A) Fe-doped $\alpha\text{-Ni(OH)}_2\text{-120}$ and B) Fe-doped $\beta\text{-Ni(OH)}_2\text{-240}$ at different scan rates in 1 M KOH in the non-faradaic potential region. C) C_{dl} of Fe-doped $\alpha\text{-Ni(OH)}_2\text{-120}$ and Fe-doped $\beta\text{-Ni(OH)}_2\text{-240}$.

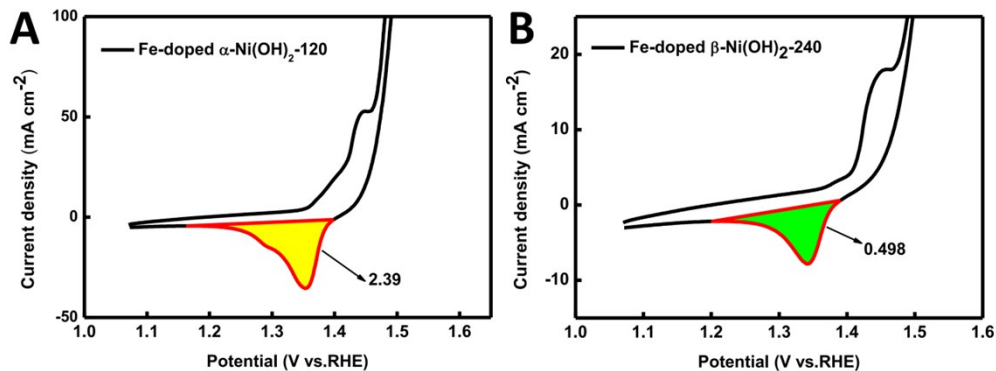


Figure S10 The reduction peak areas of Ni^{2+} to $\text{Ni}^{3+}/\text{Ni}^{4+}$ for A) Fe-doped $\alpha\text{-Ni(OH)}_2\text{-120}$ and B) Fe-doped $\beta\text{-Ni(OH)}_2\text{-240}$.

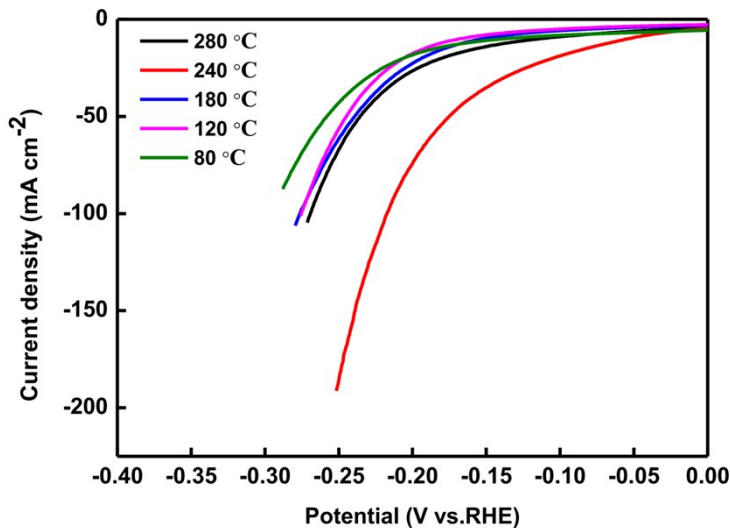


Figure S11 LSV curves of different samples prepared at different temperatures. The best HER performance is obtained at 240 °C.

Table S4 Comparisons of HER performances of Fe-doped β -Ni(OH)₂-240 with other non-precious metal HER catalysts in 1.0 M KOH.

Catalysts	j (mA cm ⁻²)	Overpotential (mV)	Ref.
NiFeOF	10	253	2
Fe-CoP	10	78	3
NiFe LDH@NiCoP	10	120	6
Ni ₃ FeN	10	158	7
Fe-Ni ₃ C	10	178	9
NiCo ₂ P _x	10	58	10
O-Co ₂ P	10	160	11
Ni ₂ P	10	176	12
NiFe-MOF	10	134	13
Mo-Ni ₂ P	10	78	14
NiO with oxygen vacancies	10	110	15
Mesoporous FeS ₂	10	96	16
CoO _x @CN	10	85	17
MoS ₂ /Ni ₃ S ₂	10	110	18
VOOH	10	164	19
MoS ₂ /Ti ₃ C ₂ -MXene@C	10	135	20
Cu@CoS _x	10	134	21
EG/H-Co _{0.85} Se P	10	150	22
Co _{0.9} S _{0.58} P _{0.42}	10	141	23
Ni/NiFe	10	210	24
Fe-doped β -Ni(OH) ₂ -240	10	53.8	This work

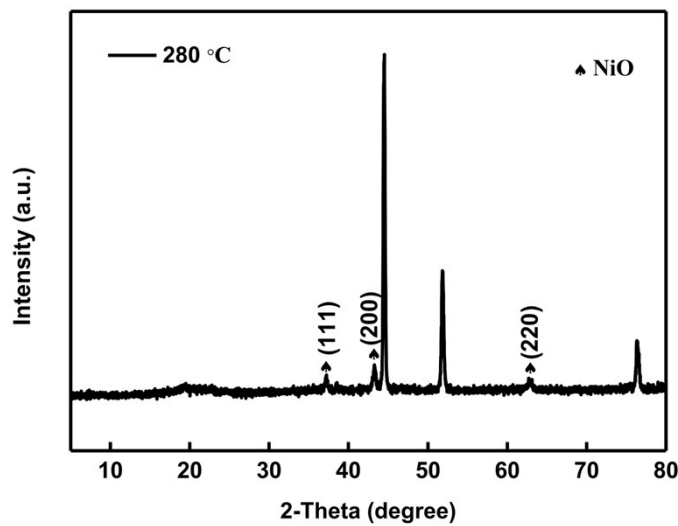


Figure S12 XRD pattern of the sample prepared at 280 °C.

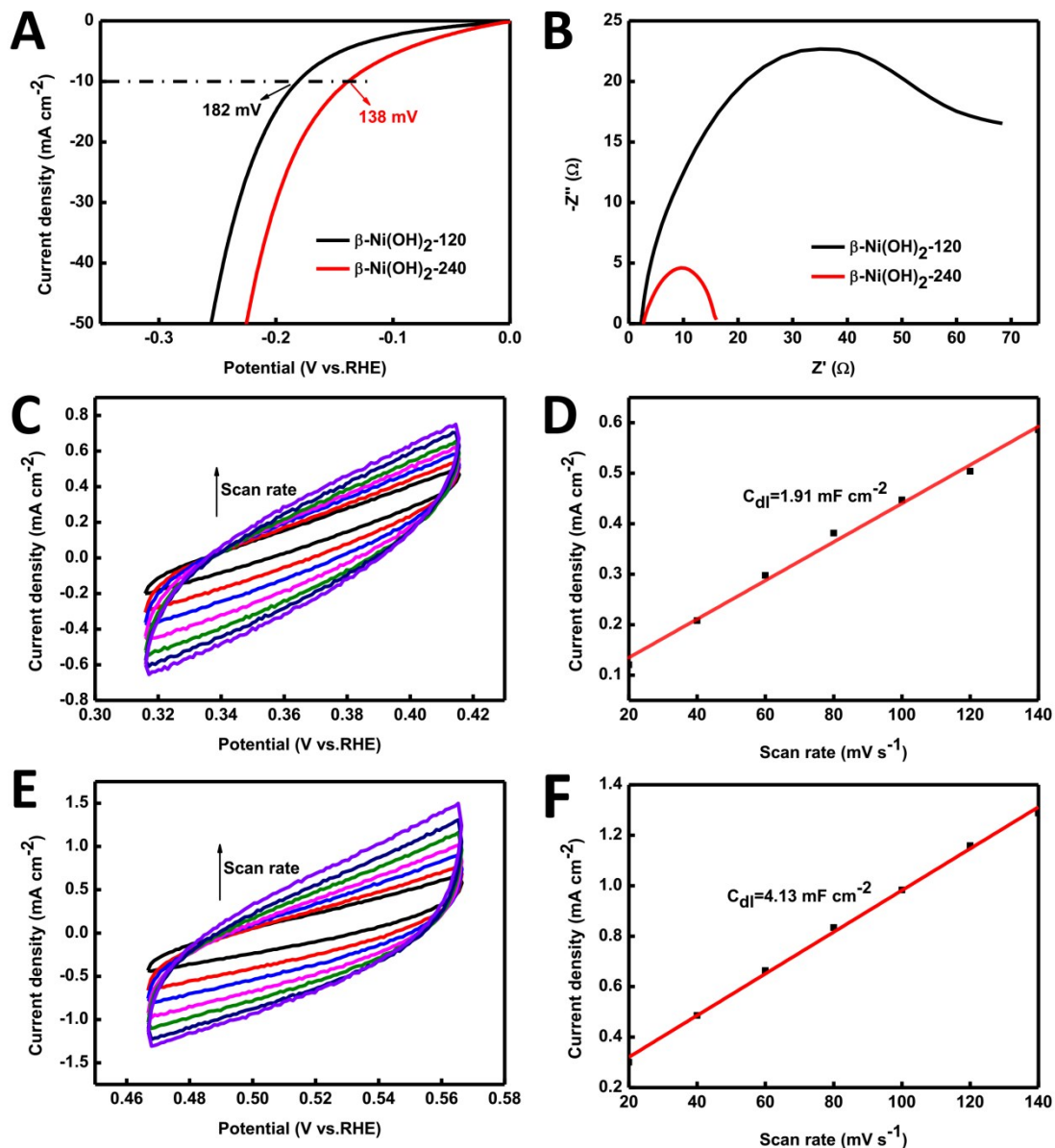


Figure S13 A) HER performance of $\beta\text{-Ni(OH)}_2$ -120 and $\beta\text{-Ni(OH)}_2$ -240 conducted in 1 M KOH. B) Nyquist plots of $\beta\text{-Ni(OH)}_2$ -120 and $\beta\text{-Ni(OH)}_2$ -240 obtained at -0.15 V vs. RHE. C) CV curves in the non-faradaic capacitance current range and D) plots of the current density versus voltage scan rate for $\beta\text{-Ni(OH)}_2$ -120. E) CV curves in the non-faradaic capacitance current range and F) plots of the current density versus voltage scan rate for $\beta\text{-Ni(OH)}_2$ -240.

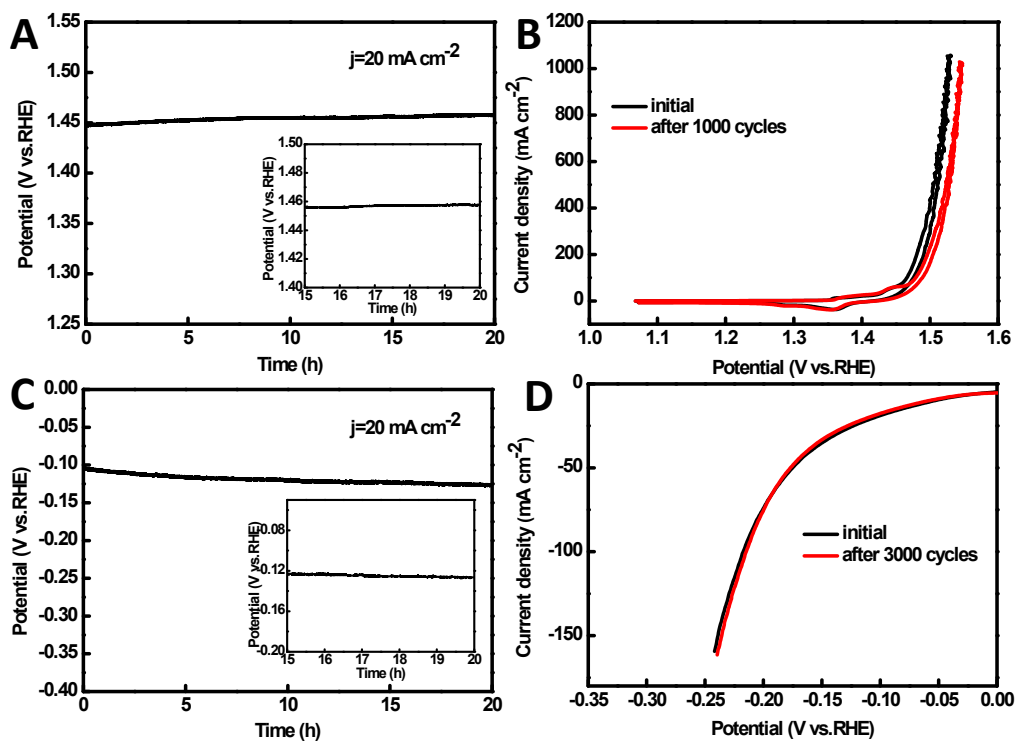


Figure S14 A) Chronopotentiometry curves ($j=20 \text{ mA cm}^{-2}$) and B) current stability testing for Fe-doped $\alpha\text{-Ni(OH)}_2$ -120 toward the OER performance. C) Chronopotentiometry curves ($j=20 \text{ mA cm}^{-2}$) and D) current stability testing for Fe-doped $\beta\text{-Ni(OH)}_2$ -240 toward the HER performance.

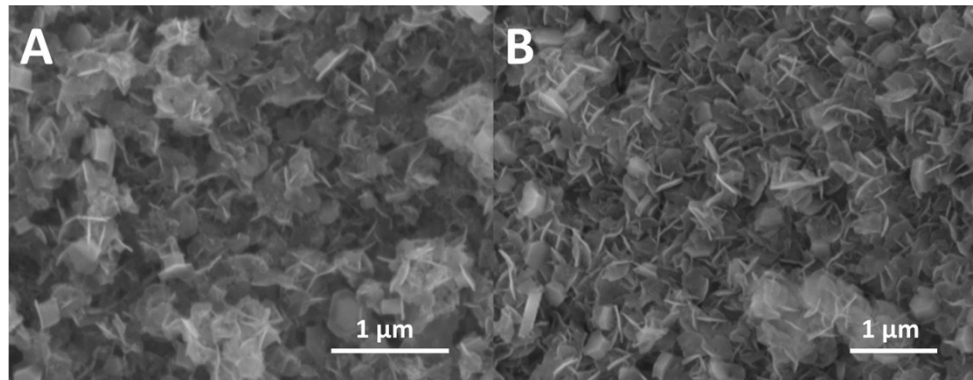


Figure S15 SEM images of Fe-doped $\beta\text{-Ni(OH)}_2$ -240 A) before and B) after the potential sweeps test.

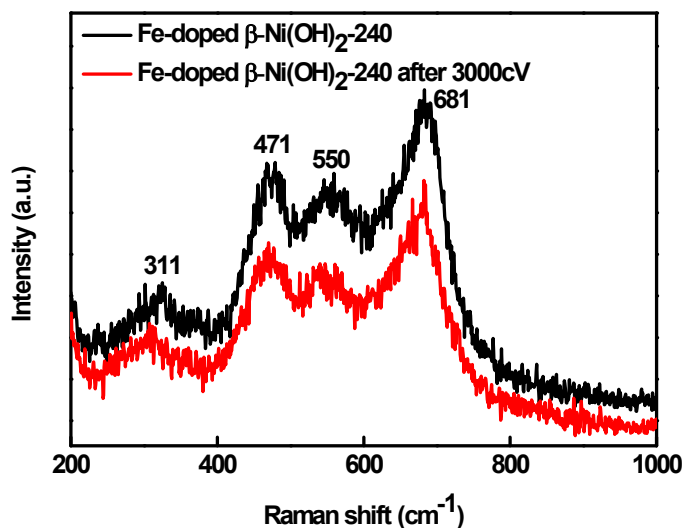


Figure S16 Raman spectra of Fe-doped β -Ni(OH)₂-240 before and after potential sweeps for 3000 cycles.

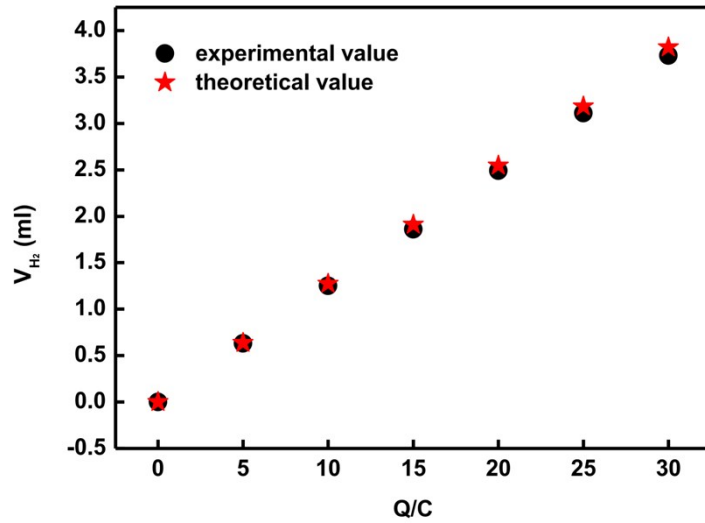


Figure S17 Quantitative H_2 measurement via water displacement.

Table S5 Structural parameters of the sample obtained from the XAFS fitting.

Catalysts	Bond type	N	R (Å)	ΔE_0 (ev)	$\sigma^2 \times 10^3$ (\AA^2)
Fe-doped α -Ni(OH) ₂ -120-Ni	Ni-O	6.7	2.03(± 0.02)	6.1(± 0.9)	8.2(± 1.2)
	Ni-Ni/Fe	6.0	3.09(± 0.03)	0.4(± 1.2)	8.6(± 0.5)
Fe-doped α -Ni(OH) ₂ -120-Fe	Fe-O	6.0(± 0.8)	1.97(± 0.09)	2.1(± 1.9)	8.5(± 2.1)
	Fe-Fe/Ni	5.9(± 1.4)	3.12(± 0.01)	9.0(± 2.0)	9.2(± 2.4)
Fe-doped β -Ni(OH) ₂ -240-Ni	Ni-O	6.5	2.04(± 0.01)	4.3(± 2.0)	8.8(± 1.1)
	Ni-Ni/Fe	5.5	3.06(± 0.02)	0.3(± 2.9)	11.0(± 0.1)
Fe-doped β -Ni(OH) ₂ -240-Fe	Fe-O	5.5(± 1.0)	1.95(± 0.01)	2.9(± 2.5)	8.1(± 2.8)
	Fe-Fe/Ni	6.0	3.11(± 0.02)	8.3(± 2.3)	9.3(± 1.1)

N, coordination number; R, distance between absorber and backscatter atoms; ΔE_0 , inner potential correction to account for the difference in the inner potential between the sample and the reference compound. σ^2 , Debye–Waller factor.

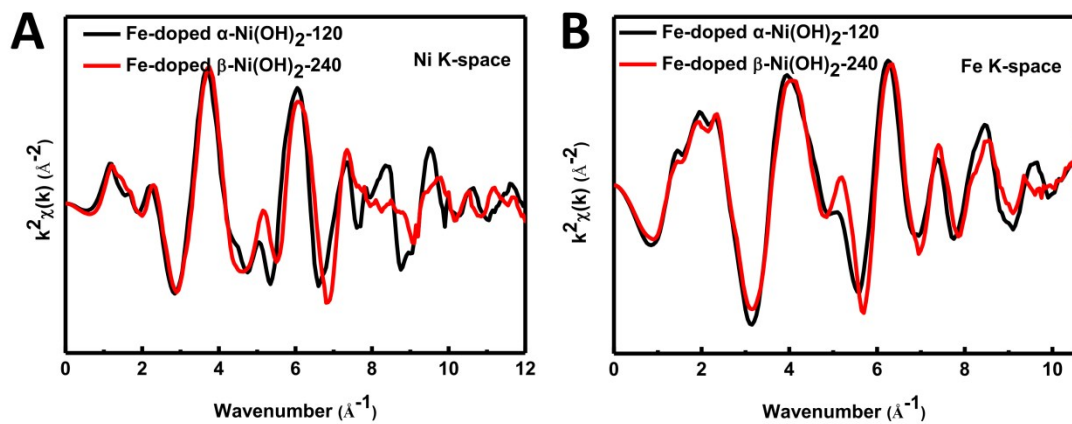


Figure S18 K-space data of the A) Ni K-edge and B) Fe K-edge for Fe-doped α -Ni(OH)₂-120 and Fe-doped β -Ni(OH)₂-240.

Table S6 . The calculated free energies of H₂O adsorption, H adsorption and H₂ adsorption for β-Ni(OH)₂, Fe-doped α-Ni(OH)₂ and Fe-doped β-Ni(OH)₂.

Catalysts	Step1: surface+2H ₂ O	Step2: surface+H ₂ O*+H ₂ O	Step3: surface+H*+OH+H ₂ O	Step4: surface+H ₂ *+2OH
β-Ni(OH) ₂				
	E=-416.09332 eV	E= -415.03170 eV	E= -415.922196 eV	E= -415.48127 eV
Fe-doped α-Ni(OH) ₂				
	E=-417.47017 eV	E= -415.60024 eV	E= -417.59544 eV	E=-417.06779 eV
Fe-doped β-Ni(OH) ₂				
	E= -418.58416 eV	E= -417.66754 eV	E=-418.80949 eV	E=-418.21136 eV

Table S7 Calculation of hydrogen adsorption energies at different sites for β-Ni(OH)₂, Fe-doped α-Ni(OH)₂ and Fe-doped β-Ni(OH)₂.

Catalysts	Active site	E(surface+H)	E(surface)	E(H ₂)	ΔE	ΔG
β-Ni(OH) ₂	Ni	-390.6912732	-387.4481224	-6.76489	0.139294	0.37929
Fe-doped α-Ni(OH) ₂	Ni	-393.1936532	-389.9389626	-6.76489	0.127754	0.36775
	Fe	-393.5785695	-389.9389626	-6.76489	-0.25716	-0.01716
Fe-doped β-Ni(OH) ₂	Ni	-392.0243956	-388.8249673	-6.76489	0.18302	0.42302
	Fe	-392.3645156	-388.8249673	-6.76489	-0.15710	0.08290

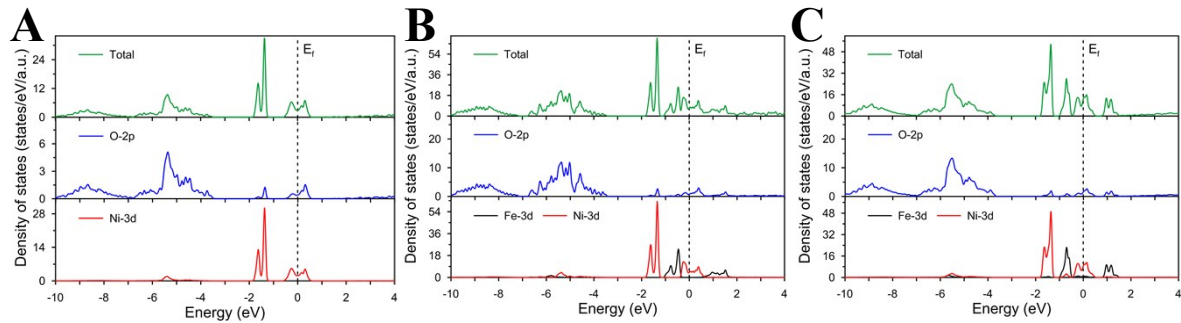


Figure S19 The calculated density of states of A) β -Ni(OH)₂, B) Fe-doped α -Ni(OH)₂ and C) Fe-doped β -Ni(OH)₂.

Table S8 Comparisons of overall water-splitting performance of Fe-doped α -Ni(OH)₂-120||Fe-doped β -Ni(OH)₂-240 with other non-nobel-metal bifunctional catalysts in 1.0 M KOH.

Catalysts	j (mA cm ⁻²)	Overpotential (mV)	Ref.
CoNi(OH) _x NiN _x	11	420	1
NiFeOF NiFeOF	10	600	2
Fe-CoP Fe-CoP	10	370	3
NiFe LDH@NiCoP NiFe LDH@NiCoP	10	340	6
Ni ₃ S ₂ Ni ₃ S ₂	13	530	8
Ni ₂ P Ni ₂ P	10	350	12
EG/H-Co _{0.85} Se P EG/H-Co _{0.85} Se P	10	410	22
NiFe-MOF NiFe-MOF	10	320	13
MoS ₂ /Ni ₃ S ₂ MoS ₂ /Ni ₃ S ₂	10	330	18
VOOH VOOH	10	390	19
Cu@CoS _x Cu@CoS _x	100	570	21
Ni/NiFe Ni/NiFe	10	330	24
NiCoP NiCoP	10	350	25
CoP CoP	10	350	26
NiSe NiSe	10	400	27
Ni ₅ P ₄ Ni ₅ P ₄	10	470	28
NiCo ₂ O ₄ /Ni ₂ P NiCo ₂ O ₄ /Ni ₂ P	10	360	29
Am FePO ₄ Am FePO ₄	10	310	30
Ni@NC Ni@NC	10	370	31
NiCoP/rGO NiCoP/rGO	10	360	32
Ni _{0.9} Fe _{0.1} /NC Ni _{0.9} Fe _{0.1} /NC	10	350	33
FeB ₂ FeB ₂	10	340	34
Ni ₃ FeN/r-GO Ni ₃ FeN/r-GO	10	370	35
Fe-doped α -Ni(OH) ₂ -120 Fe-doped β -Ni(OH) ₂ -240	10/100	290/460	This work

References

- [1] S. Li, Y. Wang, S. Peng, L. Zhang, A. M. Al-Enizi, H. Zhang, X. Sun, G. Zheng, *Adv. Energy Mater.* **2016**, *6*, 1501661.
- [2] K. Liang, L. Guo, K. Marcus, S. Zhang, Z. Yang, D. E. Perea, L. Zhou, Y. Du, Y. Yang, *ACS Catal.* **2017**, *7*, 8406-8412.
- [3] C. Tang, R. Zhang, W. Lu, L. He, X. Jiang, A. M. Asiri, X. Sun, *Adv. Mater.* **2017**, *29*, 1602441.
- [4] Q. Zhang, C. Zhang, J. Liang, P. Yin, Y. Tian, *ACS Sustainable Chem. Eng.* **2017**, *5*, 3808-3818.
- [5] Q. Liang, L. Zhong, C. Du, Y. Luo, Y. Zheng, S. Li, Q. Yan, *Nano Energy* **2018**, *47*, 257-265.
- [6] H. Zhang, X. Li, A. Hähnel, V. Naumann, C. Lin, S. Azimi, S. L. Schweizer, A. W. Maijenburg, R. B. Wehrspohn, *Adv. Funct. Mater.* **2018**, *28*, 1706847.
- [7] X. Jia, Y. Zhao, G. Chen, L. Shang, R. Shi, X. Kang, G. I. N. Waterhouse, L.-Z. Wu, C.-H. Tung, T. Zhang, *Adv. Energy Mater.* **2016**, *6*, 1502585.
- [8] L. L. Feng, G. Yu, Y. Wu, G. D. Li, H. Li, Y. Sun, T. Asefa, W. Chen, X. Zou, *J. Am. Chem. Soc.* **2015**, *137*, 14023-14026.
- [9] H. Fan, H. Yu, Y. Zhang, Y. Zheng, Y. Luo, Z. Dai, B. Li, Y. Zong, Q. Yan, *Angew. Chem., Int. Ed.* **2017**, *56*, 12566-12570.
- [10] R. Zhang, X. Wang, S. Yu, T. Wen, X. Zhu, F. Yang, X. Sun, X. Wang, W. Hu, *Adv. Mater.* **2017**, *29*, 1605502.
- [11] K. Xu, H. Ding, M. Zhang, M. Chen, Z. Hao, L. Zhang, C. Wu, Y. Xie, *Adv. Mater.* **2017**, *29*, 1606980.
- [12] P. W. Menezes, A. Indra, C. Das, C. Walter, C. Göbel, V. Gutkin, D. Schmeißer, M. Driess, *ACS Catal.* **2016**, *7*, 103-109.
- [13] J. Duan, S. Chen, C. Zhao, *Nat. commun.* **2017**, *8*, 15341.
- [14] Y. Sun, L. Hang, Q. Shen, T. Zhang, H. Li, X. Zhang, X. Lyu, Y. Li, *Nanoscale* **2017**, *9*, 16674-16679.
- [15] T. Zhang, M.-Y. Wu, D.-Y. Yan, J. Mao, H. Liu, W.-B. Hu, X.-W. Du, T. Ling, S.-Z. Qiao, *Nano Energy* **2018**, *43*, 103-109.
- [16] R. Miao, B. Dutta, S. Sahoo, J. He, W. Zhong, S. A. Cetegen, T. Jiang, S. P. Alpay, S. L. Suib, *J. Am. Chem. Soc.* **2017**, *139*, 13604-13607.
- [17] H. Jin, J. Wang, D. Su, Z. Wei, Z. Pang, Y. Wang, *J. Am. Chem. Soc.* **2015**, *137*, 2688-2694.
- [18] J. Zhang, T. Wang, D. Pohl, B. Rellinghaus, R. Dong, S. Liu, X. Zhuang, X. Feng, *Angew. Chem., Int. Ed.* **2016**, *55*, 6702-6707.
- [19] H. Shi, H. Liang, F. Ming, Z. Wang, *Angew. Chem., Int. Ed.* **2017**, *56*, 573-577.
- [20] X. Wu, Z. Wang, M. Yu, L. Xiu, J. Qiu, *Adv. Mater.* **2017**, *29*, 1607017.
- [21] Y. Liu, Q. Li, R. Si, G.-D. Li, W. Li, D.-P. Liu, D. Wang, L. Sun, Y. Zhang, X. Zou, *Adv. Mater.* **2017**, *29*, 1606200.
- [22] Y. Hou, M. Qiu, T. Zhang, X. Zhuang, C.-S. Kim, C. Yuan, X. Feng, *Adv. Mater.* **2017**, *29*, 1701589.
- [23] Z. Dai, H. Geng, J. Wang, Y. Luo, B. Li, Y. Zong, J. Yang, Y. Guo, Y. Zheng, X. Wang, Q. Yan, *ACS Nano* **2017**, *11*, 11031-11040.
- [24] Z. Wu, Z. Wang, F. Geng, *ACS Appl. Mater. Interfaces* **2018**, *10*, 8585-8593.
- [25] H. Liang, A. N. Gandi, D. H. Anjum, X. Wang, U. Schwingenschlogl, H. N. Alshareef, *Nano*

- Lett.* **2016**, *16*, 7718-7725.
- [26] W. Li, X. Gao, D. Xiong, F. Xia, J. Liu, W. G. Song, J. Xu, S. M. Thalluri, M. F. Cerqueira, X. Fu, L. Liu, *Chem. sci.* **2017**, *8*, 2952-2958.
- [27] C. Tang, N. Cheng, Z. Pu, W. Xing, X. Sun, *Angew. Chem., Int. Ed.* **2015**, *54*, 9351-9355.
- [28] M. Ledendecker, S. Krick Calderon, C. Papp, H. P. Steinruck, M. Antonietti, M. Shalom, *Angew. Chem., Int. Ed.* **2015**, *54*, 12361-12365.
- [29] L. Wang, C. Gu, X. Ge, J. Zhang, H. Zhu, J. Tu, *Adv. Mater. Interfaces* **2017**, *4*, 1700481.
- [30] L. Yang, Z. Guo, J. Huang, Y. Xi, R. Gao, G. Su, W. Wang, L. Cao, B. Dong, *Adv. Mater.* **2017**, *29*, 1704574.
- [31] Y. Xu, W. Tu, B. Zhang, S. Yin, Y. Huang, M. Kraft, R. Xu, *Adv Mater* **2017**, *29*, 1605957.
- [32] J. Li, M. Yan, X. Zhou, Z.-Q. Huang, Z. Xia, C.-R. Chang, Y. Ma, Y. Qu, *Adv. Funct. Mater.* **2016**, *26*, 6785-6796.
- [33] X. Zhang, H. Xu, X. Li, Y. Li, T. Yang, Y. Liang, *ACS Catal.* **2015**, *6*, 580-588.
- [34] H. Li, P. Wen, Q. Li, C. Dun, J. Xing, C. Lu, S. Adhikari, L. Jiang, D. L. Carroll, S. M. Geyer, *Adv. Energy Mater.* **2017**, *7*, 1700513.
- [35] Y. Gu, S. Chen, J. Ren, Y. A. Jia, C. Chen, S. Komarneni, D. Yang, X. Yao, *ACS Nano* **2018**, *12*, 245-253.